Published in final edited form as:
Org Biomol Chem. 2013 October 14; 11(38): . doi:10.1039/c3ob40870a.

Assessing the differential action on cancer cells of LDH-A inhibitors based on the *N*-hydroxyindole-2-carboxylate (NHI) and malonic (Mal) scaffolds†

Carlotta Granchi[a], **Emilia C. Calvaresi**[b], **Tiziano Tuccinardi**[a], **Ilaria Paterni**[a], **Marco Macchia**[b], **Adriano Martinelli**[a], **Paul J. Hergenrother**[b,c], and **Filippo Minutolo**[a]

[a]Dipartimento di Farmacia, Università di Pisa, Via Bonanno 6, I-56126 Pisa, Italy; filippo.minutolo@farm.unipi.it.

[b]Department of Biochemistry, University of Illinois, Urbana, Illinois 61801; hergenro@uiuc.edu.

[c]Department of Chemistry, University of Illinois, Urbana, Illinois 61801; hergenro@uiuc.edu.

Abstract

A head-to-head study of representative examples of *N*-hydroxyindole-2-carboxylates (NHI) and malonic derivatives (Mal) as LDH-A inhibitors was conducted, comparing enzyme inhibition potency, cellular uptake, reduction of lactate production in cancer cells and anti-proliferative activity. Among the compounds tested, methyl 1-hydroxy-6-phenyl-4-(trifluoromethyl)-1*H*-indole-2-carboxylate (**2**, NHI-2), a methyl ester belonging to the NHI class, displayed optimal properties in the cell-based assays, proving to be an efficient anti-glycolytic agent against cancer cells.

Introduction

Inhibition of lactate dehydrogenase (LDH) as a potential strategy for cancer treatment was proposed as early as in 1960 by Luigi Fiume,[1] in accordance with Otto Warburg's observation that cancer cells have a high consumption of glucose and produce large amounts of lactate.[2] Several decades later, anti-glycolytic therapeutic approaches against cancer have been re-evaluated, in consideration of the dependence that cancer cells have on a high glycolytic rate.[3] In particular, human LDH-A (LDH-5), a tetrameric isoform composed of four LDH-M subunits, is currently being considered as a strategic target for the blockage of glycolysis. The genetic knockdown of LDH-A has reduced the viability and invasiveness of tumor cells in several cell culture and in vivo models of breast,[4] lung,[5] esophageal,[6] and hepatocellular carcinomas.[7] People carrying a hereditary lack of the *ldh-A* gene and, therefore, completely lack any LDH-A protein, are healthy, only showing myoglobinuria after intense anaerobic exercise.[8] Thus, inhibition of LDH-A as an anticancer strategy should give no significant on-target side effects. In addition to gossypol (a nonselective inhibitor of various LDH isoforms[9]), several small molecules have been reported to inhibit LDH-A, including FX-11 (a 2,3-dihydroxy-1-naphthoic acid derivative),[10] and galloflavin.[11]

†Electronic Supplementary Information (ESI) available: [NMR spectra of **5**, HRMS of **5**, LC-UV/LC-MS chromatograms, calibration curves of **1**-**5**, docking analysis of **4** and **5**, lysate and media stability of **2** and **4**, cell culture properties of **5**]. See DOI: 10.1039/b000000x/

More recently, a series of malonic derivatives (Mal) were discovered by an elegant fragment-based approach at AstraZeneca UK,[12] which produced the first sub-micromolar inhibitors of LDH-A. Representative Mal-derivative AZ-33 (Fig. 1) inhibits LDH-A with an IC_{50} of 0.5 μM, although it is inactive in cell-based assays.[12] Other potent LDH-A inhibitors were discovered at ARIAD Pharmaceuticals, by means of a similar fragment-growing workflow starting from two terminal nicotinic acid portions.[13] With both the AstraZeneca and ARIAD compounds, the authors report limited cellular activities due to the presence of two COOH groups in the structure of the active inhibitors, which presumably could be improved either by a prodrug strategy (introduction of a double methyl ester),[12] or by the removal of one of the two COOH groups.[13]

In 2011 our research group reported the discovery of an original class of LDH-A inhibitors based on the *N*-hydroxyindole-2-carboxylate (NHI) scaffold. NHI-derivative **1** (NHI-1, Fig. 1) displayed an interesting inhibitory activity against LDH-A in the low micromolar range.[14] To further understand the differential effects that NHI and Mal derivatives may exert on cancer cells, we have now conducted a comparative study of representative "COOH"-compounds **1** (NHI-1) and **3** (AZ-33). We have then extended our investigations to methyl esters **2** (NHI-2) and **4**, since these esters may be considered as the more cell-permeable mimics or prodrugs[12] of their analogs **1** and **3**, respectively (Fig. 1). In this article, we report the results obtained in head-to-head tests conducted with both NHI and Mal derivatives, comparing: *a)* enzyme inhibition assays on LDH-A and LDH-B isoforms; *b)* intracellular accumulation; *c)* reduction of lactate production in cancer cells; and *d)* anticancer potency. Monoester **5** (Fig. 1) was found to be involved in the mechanism of activation of **4**, as explained in the following paragraphs.

Results and Discussion

In vitro inhibition of LDH-A and LDH-B

NHI and Mal derivatives **1**-**4** were assayed on LDH-A and LDH-B purified isoforms, to determine their inhibition potencies and isoform selectivities in competition experiments *vs.* both the cofactor (NADH) and the substrate (Pyr). The IC_{50} values obtained are reported in Table 1.

An NADH-competition assay with LDH-A confirmed Mal derivative **3** as the most potent inhibitor, with an IC_{50} value (0.54 μM) comparable to that reported in the literature (0.5 μM).[12] Similarly, the lack of inhibitory potency by its methyl ester **4** was also found in all our assays. On the other hand, NHI derivative **1** was confirmed to be a moderately potent LDH-A inhibitor, although considerably less potent than **3**, displaying an IC_{50} value of 29.0 μM under these conditions. Furthermore, we were pleased to find a direct inhibitory activity of NHI methyl ester **2**, with an IC_{50} value of 14.7 μM. We also assayed the novel COOMe/COOH Mal-derivative **5**, which was independently synthesized and characterized (see Experimental and Fig. S1-S3). This compound will be later discussed as the supposedly active metabolite of **4** (see Scheme 1 and discussion below). Unlike diester **4**, compound **5** displayed a very good inhibitory potency on LDH-A (IC_{50} = 4.8 μM), although inferior to that found with diacid **3**, which supports its active role in the cellular activity associated to administration of cell-permeable but inactive Mal-derivative **4**. A parallel ranking of inhibitory potencies of these compounds was confirmed in the Pyr-competition experiments, with the only exception being that **2** (10.5 μM) was more active than **5** (22.7 μM). Inhibitory assays against isoform LDH-B showed a selectivity pattern that is similar for all the active inhibitors, with a 4 to 7-fold LDH-A/LDH-B selectivity associated to both NHI derivatives (**1** and **2**) and Mal-derivatives (**3** and **5**). In addition, we applied the mixed-model inhibition fit to the second order polynomial regression analysis of the rate of conversion of NADH to

NAD^+, to obtain K_i values in the NADH-competition experiments.[15] These experiments produced an apparent Michaelis Menten constant (K_M) of 20 μM and K_i values which are consistent with the IC_{50} values reported in Table 1 for the same compounds. Here again, Mal-derivative **3** confirmed its excellent and competitive inhibition potency (K_i = 0.23 μM). Under the same conditions, NHI-derivative **1** showed a K_i value of 10.8 μM, comparable to the value we had previously obtained by the analysis of the Lineweaver-Burk plot (K_i = 8.9 μM).[14]

Molecular modelling

Molecular modelling studies were conducted to explore the binding interactions of NHIs with the target protein. Compound **2** was docked into the minimized average structure of LDH-A obtained after a computational analysis of the interactions of compound **1** with the enzyme (PDB code: 1I10).[14] The LDH-A complexes resulting from the docking of both **1**[14] and **2** were subjected to 10 ns of molecular dynamics (MD) simulations. Even after MD simulation, the carboxylic group of compound **1** maintained its polar interactions with R169 and T248, and the *N*-hydroxy group displayed a water-mediated H-bond with H193 (Fig. 2A).

The indole central scaffold of **1** was placed in a cleft delineated by H193, G194, A238, V241, I242, T248, whereas the 6-phenyl substituent was directed toward the entrance of the enzyme cavity. MD simulation of the complex with **2** highlighted a ~30° rotation along the axis perpendicular to the main plane of the molecule when the COOH group of **1** is replaced by COOMe (compare Fig. 2A and 2B). The ester group of **2** forms an H-bond with R169, whereas the methyl substituent is directed toward lipophilic residue V235. Interestingly, the rotation of the molecule leads to the formation of a new water-mediated interaction between the *N*-hydroxy group and the NH of R169, and this interaction proved to be stable during the whole MD process. This spatial shift of the molecules places the electronegative terminal portion of the CF_3-group in closer proximity to the positively charged residue R106, with the plausible formation of an additional polar interaction between **2** and the enzyme. The rest of the molecule showed interactions similar to those found with **1**, including the water-mediated H-bond between the N-OH group and H193 (Fig. 2B). The two MD trajectories were further analyzed through the combined Molecular Mechanics/Generalized Born Surface Area (MM_GBSA) approach,[16] which was proved to accurately estimate the ligand-receptor energy interaction.[17] This approach averages contributions of gas-phase energies and solvation free energies, calculated for snapshots of the complexed molecule as well as the unbound components extracted from MD trajectories according to the procedure fully described in the Supporting Information. The analysis of the interaction energies confirmed the similarity of the binding affinity of compounds **1** and **2**, with a preference for ester derivative **2**, since the MM_GBSA calculations resulted in a total interaction energy of −21.2 kcal/mol for **1** and of −24.6 kcal/mol for **2**. A docking analysis for compounds **4** and **5** suggested that the esterification of the malonic portion of **3** caused a slight (**5**) or considerable (**4**) loss of the interactions with the two arginine residues R106 and R169 in the substrate binding site of the enzyme (Fig. S4).

Cellular uptake

We determined the intracellular concentrations of NHI and Mal derivatives in HeLa cervical carcinoma cells, by treating cells with 500 μM concentrations of **1**-**4** for 30 minutes, after which cell lysates were subjected to LC-MS analysis. The relative amounts of each compound present in the intracellular fraction were detected by LC-MS. Integration areas in the UV trace at 254 nm were converted to concentration using equations generated from previous calibration of known concentrations of each compound (Fig. S5). The

experimentally-determined intracellular concentrations of compounds **1**-**4** following 500 μM incubation in whole cells, relative to compound 1, are shown in Fig. 3.

Among the NHI derivatives, concentration of methyl ester **2** in the HeLa cell lysate solution was ~4-fold higher than that of free acid **1**. No cleavage of methyl ester **2** to free acid **1** was observed following cellular incubation (Fig. S6). Diacid **3** of the Mal-class could not be detected in lysate, thus confirming the poor cellular activity previously associated to this compound.[12] On the other hand, Mal-dimethyl ester **4** showed an efficient cell uptake, similar to NHI-ester **2**, although a large second peak of MW = 511 *m/z* was detected. This additional compound was confirmed through independent chemical synthesis (Fig. S1-S3) and further testing (Fig. S7) to be monoester/monoacid **5**, which we found is formed in the cell or cell lysate after hydrolysis of a single ester group (Scheme 1 and Fig. S8-S9). The overall amount of compound **4** shown in Fig. 3 takes into account the total amount of the parent compound and that of its metabolite **5**. It is worth noting that no direct cell uptake of **5** was observed when HeLa cells were treated with a 500 μM concentration of this compound for 30 minutes (Fig. S10).

Additional experiments demonstrated that Mal-diester **4** underwent a substantial (~50%) monohydrolysis to monoester **5** upon incubation for 30 min at 37 °C in HeLa cell lysate (Fig. S8), whereas it proved to be stable in culture media (Fig. S9). Therefore, **4** should be considered as a prodrug of monoester **5**, rather than of diacid **3**.[12] Malonic diesters are known to readily undergo a first hydrolysis to monoesters, which are resistant to a second hydrolysis step, and this peculiarity is widely exploited in synthetic chemistry.[18] In addition, dimethyl esters were recently found to be unsuitable prodrugs of other bioactive malonic derivatives,[19] consistent with our findings. On the other hand, NHI-ester **2** is not cleaved to its acid analogue **1** in either cell lysate or culture media under the same conditions (Fig. S6).

Reduction of cellular lactate production

Both NHI (**1**,**2**) and Mal (**3**,**4**) derivatives were assayed for their ability to inhibit the production of lactate in cancer cells. HeLa cells were treated for 8 hours with various concentrations of the tested compounds, and the amount of lactate that formed in the cell culture media was determined by GC-MS. This GC-MS analysis of cell culture media for the quantitative determination of extracellular lactate has several-fold increased sensitivity over the ^{13}C NMR-based assay that we had previously utilized;[14] in fact it is suitable for the more accurate determination of low micromolar lactate concentrations, whereas the ^{13}C NMR method could only detect low millimolar concentrations of the same metabolite. As shown in Fig. 4, NHI-acid **1** caused a modest reduction of lactate production relative to vehicle (down to 70% at 100 μM), consistent with previous results.[14] A much more efficient and dose-dependent reduction was displayed by its methyl ester **2**, which proved to be the most effective inhibitor of lactate production at the maximum concentration utilized (down to ~20% at 200 μM). This potent inhibition of cell lactate production attained with methyl ester **2** is likely due to its several-fold enhanced cell uptake compared to its acid **1**. Among the Mal-derivatives, free acid **3** did not show any effect on the production of lactate, consistent with its demonstrated poor cell permeability, whereas its ester analog **4** caused a significant reduction, presumably due to its conversion to the active LDH-A inhibitor **5** in cells. However, 8 hour treatment of HeLa cells with up to 200 μM concentrations of monoester **5** (Fig. S11b) in agreement with its negligible cellular uptake. The potencies of compounds **1** and **2** up to 200 μM concentrations of monoester **5** failed to result in any substantial reduction in lactate production (Fig. S11a), thus confirming the poor cell permeability of **5** described above (Fig. S10).

Inhibition of cancer cell proliferation

The growth inhibitory effect of these compounds was assessed by exposing HeLa cells for 72 hours to varying concentrations of **1-5**, after which cell death was assessed by Sulforhodamine B staining, as previously described.[20] The anticancer potencies of compounds **1-4** expressed as IC_{50} values (the concentration of compound required to kill 50% of cells, where lower concentrations indicate increased potency), are plotted in Fig. 5 and S11b.

Compounds belonging to the NHI chemical class, such as **1** and **2**, displayed higher potencies (IC_{50} = 43.8 and 33.4 μM, respectively), than their Mal analogs. In fact, diacid **3** was found to be completely inactive (IC_{50} value > 500 μM), consistent with its poor cellular permeability. Dimethyl ester **4** showed an IC_{50} value of 75.4 μM in HeLa cells. No substantial cell death was noted in HeLa cells upon 72 hour treatment with were also preliminarily assessed in a non-cancerous immortalized cell line, WT-MEF. From this experiment, it was determined that treatment with 100 μM compound **1** resulted in less than 20% cell death at 72 hours, and treatment with 100 μM compound **2** resulted in approximately 70% cell death at 72 hours. By contrast, treatment with 100 μM of both compounds **1** and **2** in HeLa cervical carcinoma cells resulted in 100% cell death at 72 hours, thus suggesting that these NHI series compounds have reduced toxicity in non-cancerous versus cancerous cells.

Conclusion

Our comparative biological evaluations of NHI- and Mal-derivatives revealed that both chemical scaffolds may be suitable for the development of anticancer agents targeting LDH-A. Furthermore, these studies led to the discovery of the intrinsic inhibitory activity of methyl ester **2**, which does not behave as a prodrug of **1**, but instead behaves consistently with an active in vitro and cellular inhibitor of LDH-A. Conversely, dimethyl ester **4** of the Mal class undergoes a rapid mono-hydrolysis upon entrance into HeLa cells, thus producing intermediate **5**, which then inhibits LDH-A and is responsible for the cellular effects of **4**. However, while the in vitro LDH-A inhibition afforded by **5** are similar to that afforded by **2**, the cellular lactate production and anticancer potency of **2** are superior to those of **5**'s prodrug, compound **4**. Presently, the best combination of enzyme inhibition potency, cell membrane permeation, reduction of cellular lactate production, and anti-proliferative activity on cancer cells is found in NHI-derivative **2**.

Experimental

General chemistry methods

Commercially available chemicals were purchased from Sigma-Aldrich or Alfa Aesar and used without further purification. NMR spectra were obtained with a Varian Gemini 200 MHz spectrometer. Chemical shifts (δ) are reported in parts per million downfield from tetramethylsilane and referenced from solvent references. *J* values are given in Hz. Chromatographic separations were performed on silica gel columns by flash (Kieselgel 40, 0.040–0.063 mm; Merck) or gravity column (Kieselgel 60, 0.063–0.200 mm; Merck) chromatography. Reactions were followed by thin-layer chromatography (TLC) on Merck aluminum silica gel (60 F_{254}) sheets that were visualized under a UV lamp. Evaporation was performed in vacuo (rotating evaporator). Sodium sulfate was always used as the drying agent. LC-MS characterization was performed using a Waters Quattro II quadrupole-hexapole-quadrupole liquid chromatography/mass spectrometry apparatus (Waters, Milford, MA) equipped with an electrospray ionization source. LC separation was achieved using a C18 Waters Xbridge column (2.1×20mm, Waters) at 25 °C using a linear gradient of mobile

phases: 95% H_2O, 5% acetonitrile, and 0.1% formic acid (A) and 95% acetonitrile, 5% H_2O, and 0.1% formic acid (B). Solution A was initially passed through the column but decreased linearly to 50% of the mobile phase at 10 minutes and 0% of the mobile phase at 25 minutes. The flow rate was 200 μL/min, and the injection volume was 10 μL. The mass spectrometer was operated in negative mode for intracellular concentration determination experiments, and in positive mode for the collection of the high-resolution LC-MS determination of compound **5**. The ultraviolet (UV) detector was programmed to monitor absorbance at 254 nm for all runs, to detect the phenyl ring present in all compounds. 1-Hydroxy-6-phenyl-4-(trifluoromethyl)-1*H*-indol-2-carboxylic acid (**1**, NHI-1) and methyl 1-hydroxy-6-phenyl-4-(trifluoromethyl)-1*H*-indol-2-carboxylate (**2**, NHI-2) were prepared as previously reported.[14] Malonic derivatives 2-(4-(4-((3-((2-methylbenzo[*d*]thiazol-6-yl)amino)-3-oxopropyl)amino)-4-oxobutyl)benzyl)malonic acid (**3**, AZ-33) and dimethyl 2-(4-(4-((3-((2-methylbenzo[*d*]thiazol-6-yl)amino)-3-oxopropyl)amino)-4-oxobutyl)benzyl)malonate (**4**) were obtained using the literature protocol.[12]

3-Methoxy-2-(4-(4-((3-((2-methylbenzo[*d*]thiazol-6-yl)amino)-3-oxopropyl)amino)-4-oxobutyl)benzyl)-3-oxopropanoic acid (5)

To a stirring solution of dimethylester **4**[12] (40.0 mg; 0.076 mmol) in THF (0.5 mL) and H_2O (0.5 mL) at 0 °C was added $LiOH{\cdot}H_2O$ (3.2 mg; 0.076 mmol). After 2h the mixture was concentrated under vacuum, diluted with H_2O and washed with Et_2O. The aqueous phase was then acidified (1N HCl) and extracted with EtOAc. The organic phase was dried (Na_2SO_4) and concentrated by rotary evaporation to give the title compound as an off-white solid (32 mg, 83%). δ_H (200 MHz; CD_3OD) 1.85 (2 H, quintet, *J* 7.5, $-CH_2CH_2CH_2^-$), 2.18 (2 H, t, *J* 7.3, $-CH_2^-$), 2.54 (2 H, *pseudo*-t, *J* 7.7, $-CH_2^-$), 2.62 (2 H, t, *J* 6.5, $-CH_2^-$), 2.80 (3 H, s, benzothiazole-CH_3), 3.07 (2 H, d, *J* 7.9, Ar-CH_2-malonic portion), 3.50–3.60 (3 H, m, malonic C*H* + $-CH_2$-NH-C(O)-), 3.64 (3 H, s, $-COOCH_3$), 7.0–7.1 (4 H, br s, phenyl Ar-*H*), 7.47 (1 H, dd, J_o 8.8, J_m 2.2, benzothiazole H-3), 7.77 (1 H, d, J_o 8.8, benzothiazole H-4), 8.36 (1 H, d, J_m 2.0, benzothiazole H-7) [the two amide N*H*s are visible in DMSO-d_6 at 7.95 (1 H, t, *J* 5.6, - C(O)N*H*-CH_2^-) and 10.16 (1 H, s, $-C(O)NH$-Ar)]. δ_C (50 MHz; CD_3OD) 19.59 (benzothiazole 2-CH_3), 28.67 (-$CH_2CH_2CH_2^-$), 35.38 (-CH_2^-), 35.74 (-CH_2^-), 36.51 (-CH_2^-), 36.84 (-CH_2^-), 37.64 (-CH_2^-), 52.73 (-$COOCH_3$), 113.57 (benzothiazole C-7), 120.34 (benzothiazole C-5), 122.62 (benzothiazole C-4), 129.48 (2C, C^{III}, Ph), 129.68 (2C, C^{III}, Ph), 136.87, 137.18 (2C), 141.22 (C^{IV}, 2xPh, benzothiazole C-6 and C-7a), 150.49 (benzothiazole C-3a), 168.79 (benzothiazole C-2), 171.21 (C=O), 171.87 (C=O), 172.07 (C=O), 175.98 (C=O) [malonic *C*H overlaps with solvent residual peaks in CD_3OD; it is instead visible at 51.74 ppm in DMSO-d_6]. MS (ESI^-) *m/z* 510 (50, $M-H^+$), 466 (100, $M-CO_2-H^+$). HRMS (ESI^+) Calcd for $C_{26}H_{30}N_3O_6S^+$ ($M+H^+$): 512.1855. Found: 512.1850. HPLC purity >96%.

Docking procedure

Compounds **2**, **4** and-**5** were built using Maestro 9.0[21] and were minimized using the conjugate gradient method until a convergence value of 0.05 kcal/(mol·Å) was reached. The minimization was carried out in a water environment model (generalized-Born/surface-area model) using the MMFFs force field and a distance-dependent dielectric constant of 1.0. The LDH-A chain was extracted from the minimized average structure of the complex between LDH and **1** obtained by us through molecular dynamic simulations.[14]

Automated docking was carried out by means of the GOLD 5.1 program.[22] The “allow early termination” option was deactivated, the remaining GOLD default parameters were used, and the ligand was submitted to 30 genetic algorithm runs by applying the ChemScore fitness function.

MD Simulations

The best docked conformation was taken into account. The so obtained complex was energy minimized using AMBER 11.[23] The complex was placed in a rectangular parallelepiped water box, an explicit solvent model for water (TIP3P) was used, and the complex was solvated with a 10 Å water cap. Chlorine ions were added as counterions to neutralize the system. Two steps of minimization were then carried out. In the first stage, we kept the complex fixed with a position restraint of 500 kcal/(mol·Å^2) and we solely minimized the positions of the water molecules. In the second stage, we minimized the entire system through 20 000 steps of steepest descent followed by conjugate gradient until a convergence of 0.05 kcal/(mol·Å) was attained. All the a carbons of the protein were blocked with a harmonic force constant of 10 kcal/(mol·Å^2). Ten nanoseconds of MD simulation were then carried out. The time step of the simulations was 2.0 fs with a cutoff of 10 Å for the non-bonded interaction, and SHAKE was employed to keep all bonds involving hydrogen atoms rigid. Constant-volume periodic boundary MD was carried out for 400 ps, during which the temperature was raised from 0 to 300 K. Then 9.6 ns of constant pressure periodic boundary MD was carried out at 300 K using the Langevin thermostat to maintain constant the temperature of our system. General Amber force field (GAFF) parameters were assigned to the ligand, while partial charges were calculated using the AM1-BCC method as implemented in the Antechamber suite of AMBER 11. The final structure of the complex was obtained as the average of the last 8 ns of MD minimized by the CG method until a convergence of 0.05 kcal/(mol·Å). The average structure was obtained using the ptraj program implemented in AMBER 11. The same MD protocol was also applied for the already reported LDH-**1**complex, in order to obtain two MD trajectories of the two compounds starting from the same protein structure. This step has been necessary for a better evaluation of the subsequent MM-GBSA analysis.

Energy Evaluation

We extracted 80 snapshots (at time intervals of 10 ps) for each species (complex, receptor and ligand) from the last 800 ps of MD of the two ligand-LDH complexes. Electrostatic, van der Waals, and internal energies were obtained using the SANDER module in AMBER 11. Polar energies were obtained from the GBSA module of AMBER 11 program (using the Generalized-Born approximation). Nonpolar energies were evaluated separating them into two terms: the attractive (dispersion) and repulsive (cavity) interactions.

Enzyme assays

The compounds were evaluated in enzymatic assays to assess their inhibitory properties against two commercially available purified human isoforms of lactate dehydrogenase, *h*LDH5 (LDH-A4, LEEBIO - USA) and *h*LDH1 (LDH-B4, Sigma Aldrich - USA). The reaction of lactate dehydrogenase was conducted using the “forward” direction (pyruvate → lactate), and the kinetic parameters for the substrate (pyruvate) and the cofactor (NADH) were measured by fluorescence (emission wavelength at 460 nm, excitation wavelength at 340 nm), to monitor the amount of NADH consumed (for IC_{50} measurements), or the rate of conversion of NADH to NAD^+ and, therefore, the progression of the reaction (for K_i measurements).

These assays were conducted in wells containing 200 μL of a solution comprising the reagents dissolved in 100 mM phosphate buffer (KH_2PO_4 and K_2HPO_4) at pH 7.4. DMSO stock solutions of compounds were prepared (concentration of DMSO did not exceed 4% during the measurements). Assays were performed in 96-well plates. For IC_{50} calculation, seven different concentrations (in duplicate for each concentration) of compound were used to generate a concentration-response curve. In the NADH-competition assay, compounds were tested in the presence of 40 μM NADH and 1440 μM pyruvate; in pyruvate-

competition assay, compounds were tested in the presence of 150 μM NADH and 200 μM pyruvate. Compound solutions were dispensed in 96-well plates (8 μL), then substrate and cofactor dissolved in buffer (152 μL) and enzyme solution (40 μL) were added. Any possible background fluorescence of the tested compounds, or their quenching of NADH fluorescence, was subtracted. In addition to the compound test wells, each plate contained maximum and minimum controls. Assay plates were incubated for 15 min, and the final measurements were performed using Victor X3 Microplates reader (PerkinElmer®). IC_{50} values were generated using the curve-fitting tool of GraphPad Prism software (GraphPad – USA).

In the enzyme kinetics experiments, compounds were tested in the presence of scalar concentrations of NADH. They were added in scalar amounts (concentration range = 30-0.2 μM) to a reaction mix containing phosphate buffer, 1.4 mM pyruvate and scalar concentrations of NADH (9.6-60 μM). Finally, LDH solution was added (0.015 UmL^{-1}). LDH activity was measured by recording the decrease in NADH fluorescence using a Victor X3 Microplates Reader (PerkinElmer®). The experimental data were analyzed by non-linear regression analysis with GraphPad Prism software, using a second order polynomial regression analysis, by applying the mixed-model inhibition fit.[15]

Calibration, intracellular concentration assessment, and media stability by LC-MS

To correlate compound integration area with compound concentration, calibration equations for compounds **1-5** were constructed as follows. Standards containing 0, 6.25, 12.5, 25, 50, 75, and 100 μM of each compound were prepared in 1 mL methanol with 1% DMSO content in each sample. A fraction of each aliquot was analyzed via LC-MS using the instrument, column, solvent system, and running conditions described above (see General methods). This protocol achieved separation of all three compounds on both the UV trace and total ion chromatograph (TIC), with compound **3** eluting first (8.9 minutes UV), followed by compound **5** (9.7 minutes UV), compound **4** (11.0 minutes UV), compound **1** (14.1 minutes UV), and compound **2** (15.9 minutes UV). Spectra were visualized and integrated using MassLynx spectrometry software (Waters); representative spectra are shown in Figure S5a (UV trace). The UV trace was used to integrate compound concentration in all further experiments. Integration areas were plotted against compound concentration, and from these data points linear equations were calculated to represent the relationship between concentration and integration area (Fig. S5b). The mass spectral data were used to confirm the correct molecular weights for all compounds. Intracellular concentration of compounds **1-4** were then assessed in HeLa human cervical carcinoma cells (ATCC, Manassas, VA). Cells were grown to confluence in 6 well plates prior to being treated with 500 μM of compound, or vehicle control (prepared in DMSO) in 1 mL total volume (1% final concentration DMSO in all treatments). After 30 minutes of incubation at 37 °C, cells were collected by trypsinization (5 minute incubation with 0.05% trypsin + 0.53 mM EDTA in HBSS without sodium bicarbonate, calcium, or magnesium, 37 °C) and washed with sterile PBS, 37 °C. Cell pellets were then resuspended in 300 μL cold methanol and disrupted by sonication using an XL-2000 Misonix sonicator (Qsonica, Newton, CT). After a 30 minute incubation at 4 °C to facilitate precipitation of proteins, the sonicates were centrifuged, and a portion of the supernatant was analyzed by LC-MS using the acquisition parameters described previously, with the additional supernatant stored at −80 °C. The resulting UV traces were integrated at 8.9 minutes (compound **3**), 9.7 minutes (compound **5** – a cleavage product observed in treatment of cells with compound **4**), 11.0 minutes (compound **4**), 14.1 minutes (compound **1**), and 15.9 minutes (compound **2**); the UV trace of vehicle-treated sonicates from both the start and end of the experiment time course contained no peaks in this range. UV integration areas were calculated by MassLynx software. Average integration areas for each compound were calculated using values

obtained over four independent experiments. Since cleavage of compound **4** (dimethyl ester) to compound **5** (monomethyl ester) had been observed repeatedly upon incubation of compound **4** in HeLa cells, experiments were conducted to determine whether this cleavage was occurring in cell lysate or in RPMI 1640 growth media (RPMI 1640 media with 10% FBS and 1% Penstrep solution). Fresh HeLa cell lysate was obtained by pelleting 1,200,000 HeLa cells and sonicating the pellet in 800 μL growth media, warmed to 37 °C. Immediately after sonication, 198 μL aliquots of lysate were added to microfuge tubes to which 2 μL compound **2** (NHI-2) or compound **4** (both in 10 mM DMSO solutions), or DMSO vehicle, had already been added (for a final concentration of 100 μM compound after addition of lysate). Concurrently, 198 μL aliquots of growth media, warmed to 37 °C, were added to separate microfuge tubes to which 2 μL compound **2** or **4** (in 10 mM DMSO solutions), or DMSO vehicle, had already been added (for a final concentration of 100 μM compound after addition of growth media). All six samples were incubated at 37 °C for 30 minutes to mimic the conditions of the cellular experiment. Following the incubation period, 100 μL of each aliquot were obtained for LC-MS analysis using the collection protocol described previously. UV traces (at 254 nm) and mass spectra of peaks of interest in the total ion chromatographs are shown in Figs. S6-S10. Compound **2** was not appreciably cleaved in either cell culture media or HeLa cell lysate (Fig. S6). Compound **4** was not appreciably cleaved in cell culture media (Fig. S9), but it was substantially cleaved to compound **5** upon 30 minute incubation in HeLa cell lysate (Fig. S8).

Assessment of lactate production

Confluent HeLa human cervical carcinoma cells in a 96 well plate were treated with compound or vehicle control (1% DMSO final concentration) in DMEM media minus phenol red + 10% dialyzed FBS + 1% Penstrep, supplemented with 10 mM glucose, 1 mM sodium pyruvate and 4 mM glutamine, in a final volume of 125 μL per well. Immediately following compound addition, plates were incubated for 8 hours at 37 °C in a 95% air/5% CO_2 atmosphere. Duplicate wells were prepared for each treatment. Following treatment, media was collected, and 100 μL were added to 2 μL 50 mM chlorophenylalanine (CPA; internal standard for GC-MS analysis). Samples were concentrated, derivatized by a four-hour incubation with MTBSTFA + 1% TBDMCS (Thermo Scientific, Walthman, MA) in acetonitrile at 85 °C, and immediately analyzed using GC-MS (Agilent 6890N GC/5973 MS, equipped with an Agilent DB-5 capillary column, 30 M × 320 μM × 0.25 μM, model number J&W 123-5032, Agilent Technologies, Santa Clara, CA) and an electron impact ionization source. One microliter of each sample was injected using an automated injector, and a solvent delay of 8.20 minutes was implemented. The initial oven temperature was 120 °C, held for 5 minutes; then the temperature was increased at a rate of 10 °C/minute until a temperature of 250 °C was reached. Temperature was then increased by 40 °C/minute until a final temperature of 310 °C was reached. Total run time per sample was 22.5 minutes.

Compounds were identified using AMDIS Chromatogram software (Amdis) and programmed WIST and Niley commercial libraries. The integration area of lactate in each sample was divided by the integration area of CPA in the same sample to achieve a lactate/internal standard ratio. The ratios were averaged for duplicates, and percent lactate production over vehicle was calculated for each independent experiment. The mean lactate production/vehicle was then averaged between three or more independent experiments.

Assessment of anticancer potency

HeLa cells were grown in RPMI 1640 media supplemented with 10% FBS and 1% Penicillin/Streptomycin, were added at a density of 5000 cells/well to 96 well plates to which 31.6 nM-200 μM compound (for compounds **1, 2** and **5**) or 1 μM-500 μM compound (for compounds **3**and **4**) in DMSO was already added (1% final concentration DMSO in all

wells; triplicate wells at the same concentration per repetition). Plates were incubated at 37 °C in a 95% air/5% CO_2 atmosphere for 72 hours. Media was removed and cells were fixed by the addition of 50 μL 10% trichloroacetic acid in water, 4 °C, to each well. Plates were incubated at 4 °C for at least one hour, and the Sulforhodamine B (SRB) colorimetric assay was performed to assess remaining biomass in each well. Briefly, plates were washed thrice in tap water and dried before the addition of 50 μL SRB dye solution (0.057% w/v SRB in 1% glacial acetic acid) to each well. Following a 30 minute incubation, unbound dye was removed by washing each plate six times in 1% glacial acetic acid. Two hundred microliters of 10 mM Tris buffer (pH=10.5) was added to each dried well to solubilize the bound dye, and after a 30 minute incubation, absorbance of each well was read at 510 nm in a microplate reader. Cells treated with 1% DMSO were used as the 100% live control for biomass, and wells incubated with media alone were used as the baseline zero biomass control. IC_{50} values for each replicate were calculated using SoftMax Pro software (Molecular Devices, Sunnyvale, CA). Average IC_{50} values and standard error were attained by averaging data from three independent experiments. The growth inhibition potency of compounds **1** and **2** were similarly evaluated in a non-cancerous immortalized cell line, WT-MEF. Each compound (at 100 μM) was incubated with 5,000 WT-MEF cells cultured in DMEM media (+ 10% FBS + 1% Penstrep) for 72 hours at 37 °C, alongside cells treated with 1% DMSO vehicle. Cells were fixed using 10% trichloroacetic acid solution, and an SRB assay was performed to quantify remaining biomass relative to vehicle and no biomass control wells.

Supplementary Material

Refer to Web version on PubMed Central for supplementary material.

Acknowledgments

We are grateful to the NIH (R01GM098453), the University of Pisa, and the University of Illinois for funding. E.C.C. is an NIH Ruth L. Kirschstein National Research Service Award predoctoral fellow (1F30CA168323-01) and a UIUC Department of Biochemistry Herbert Carter fellow. F.M. thanks Drs. Mario Varasi, Daniele Fancelli, and Simon Plyte of the European Institute of Oncology (I.E.O.), Milano – Italy for helpful discussions, and Dr. Giorgio Placanica of the University of Pisa for technical assistance in the analysis of the products.

Notes and references

1. Fiume L. Nature. 1960; 187:792–793. [PubMed: 13823333]
2. Warburg O. Science. 1956; 123:309–314. [PubMed: 13298683]
3. Granchi C, Minutolo F. ChemMedChem. 2012; 7:1318–1350. [PubMed: 22684868]
4. Fantin VR, St-Pierre J, Leder P. Cancer Cell. 2006; 9:425–434. [PubMed: 16766262]
5. Seth P, Grant A, Tang J, Vinogradov E, Wang X, Lenkinski R, Sukhatme VP. Neoplasia. 2011; 13:60–71. [PubMed: 21245941]
6. Yao F, Zhao T, Zhong C, Zhu J, Zhao H. Tumour Biol. 2013; 34:25–31. [PubMed: 22961700]
7. Sheng SL, Liu JJ, Dai YH, Sun XG, Xiong XP, Huang G. FEBS J. 2012; 279:3898–3910. [PubMed: 22897481]
8. Kanno T, Sudo K, Maekawa M, Nishimura Y, Ukita M, Fukutake K. Clin Chim Acta. 1988; 173:89–98. [PubMed: 3383424]
9. Gomez MS, Piper RC, Hunsaker LA, Royer RE, Deck LM, Makler MT, Vander Jagt DL. Mol Biochem Parasitol. 1997; 90:235–246. [PubMed: 9497046]
10. Le A, Cooper CR, Gouw AM, Dinavahi R, Maitra A, Deck LM, Royer RE, Vander Jagt DL, Semenza GL, Dang CV. Proc Natl Acad Sci U S A. 2010; 107:2037–2042. [PubMed: 20133848]
11. Manerba M, Vettraino M, Fiume L, Di Stefano G, Sartini A, Giacomini E, Buonfiglio R, Roberti M, Recanatini M. ChemMedChem. 2012; 7:311–317. [PubMed: 22052811]

12. Ward RA, Brassington C, Breeze AL, Caputo A, Critchlow S, Davies G, Goodwin L, Hassall G, Greenwood R, Holdgate GA, Mrosek M, Norman RA, Pearson S, Tart J, Tucker JA, Vogtherr M, Whittaker D, Wingfield J, Winter J, Hudson K. J Med Chem. 2012; 55:3285–3306. [PubMed: 22417091]
13. Kohlmann A, Zech SG, Li F, Zhou T, Squillace RM, Commodore L, Greenfield MT, Lu X, Miller DP, Huang WS, Qi J, Thomas RM, Wang Y, Zhang S, Dodd R, Liu S, Xu R, Xu Y, Miret JJ, Rivera V, Clackson T, Shakespeare WC, Zhu X, Dalgarno DC. J Med Chem. 2013; 56:1023–1040. [PubMed: 23302067]
14. Granchi C, Roy S, Giacomelli C, Macchia M, Tuccinardi T, Martinelli A, Lanza M, Betti L, Giannaccini G, Lucacchini A, Funel N, Leon LG, Giovannetti E, Peters GJ, Palchaudhuri R, Calvaresi EC, Hergenrother PJ, Minutolo F. J Med Chem. 2011; 54:1599–1612. [PubMed: 21332213]
15. Copeland, RA. Enzymes: a practical introduction to structure, mechanism, and data analysis. 2nd edn.. Wiley; New York: 2000.
16. Kollman PA, Massova I, Reyes C, Kuhn B, Huo S, Chong L, Lee M, Lee T, Duan Y, Wang W, Donini O, Cieplak P, Srinivasan J, Case DA, Cheatham TE 3rd. Acc Chem Res. 2000; 33:889–897. [PubMed: 11123888]
17. Greenidge PA, Kramer C, Mozziconacci JC, Wolf RM. J Chem Inf Model. 2013; 53:201–209. [PubMed: 23268595]
18. Krapcho AP. Synthesis-Stuttgart. 1982:805–823.
19. Wilhelm A, Lopez-Garcia LA, Busschots K, Frohner W, Maurer F, Boettcher S, Zhang H, Schulze JO, Biondi RM, Engel M. J Med Chem. 2012; 55:9817–9830. [PubMed: 23106316]
20. Vichai V, Kirtikara K. Nat Protoc.
21. Schrödinger Inc; Portland, OR: 2009.
22. Verdonk ML, Cole JC, Hartshorn MJ, Murray CW, Taylor RD. Proteins. 2003; 52:609–623. [PubMed: 12910460]
23. Case, DA.; Darden, TA.; E. C., T., III; Simmerling, CL.; Wang, J.; Duke, RE.; Luo, R.; Walker, RC.; Zhang, W.; Merz, KM.; Roberts, B.; Wang, B.; Hayik, S.; Roitberg, A.; Seabra, G.; Kolossváry, I.; Wong, KF.; Paesani, F.; Vanicek, J.; Liu, J.; Wu, X.; Brozell, SR.; Steinbrecher, T.; Gohlke, H.; Cai, Q.; Ye, X.; Wang, J.; Hsieh, M-J.; Cui, G.; Roe, DR.; Mathews, DH.; Seetin, MG.; Sagui, C.; Babin, V.; Luchko, T.; Gusarov, S.; Kovalenko, A.; Kollman, PA. University of California; San Francisco, CA: 2010.

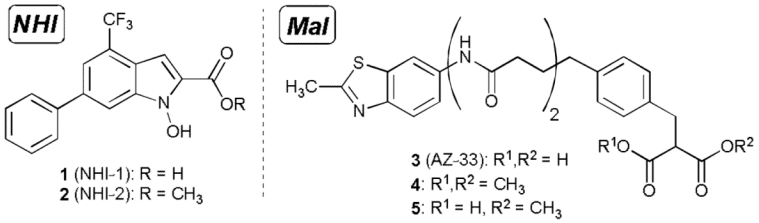

Fig 1.
Structures of NHI and Mal derivatives

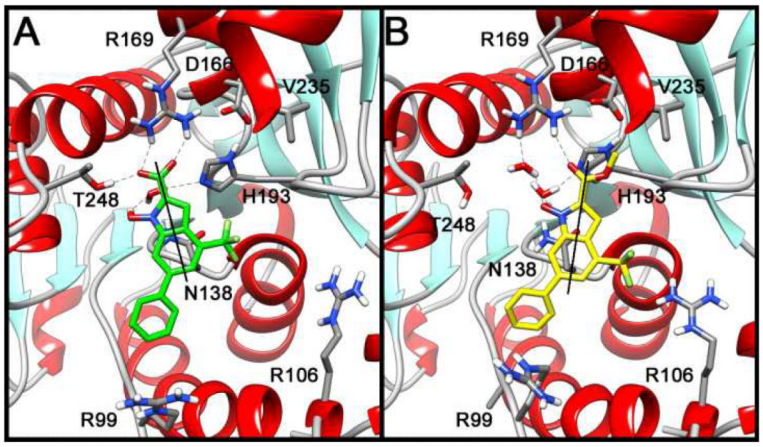

Fig 2.

Binding poses resulting from MD simulation of the LDH-A complex with **1** (A, green) and **2** (B, yellow).

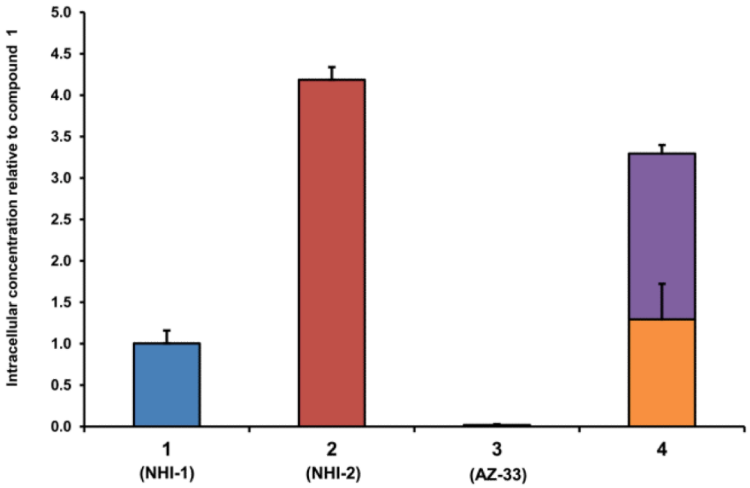

Fig 3.

Relative intracellular concentrations of compounds **1**-**4** in HeLa cells determined by LC-MS. Data are graphed relative to compound **1**. Compound **4** was substantially cleaved to compound **5** in cells. The orange bar denotes the intracellular concentration of the remaining compound **4**; the purple bar denotes the concentration of cleavage product (compound **5**). Error bars denote standard error (n=4 independent experiments).

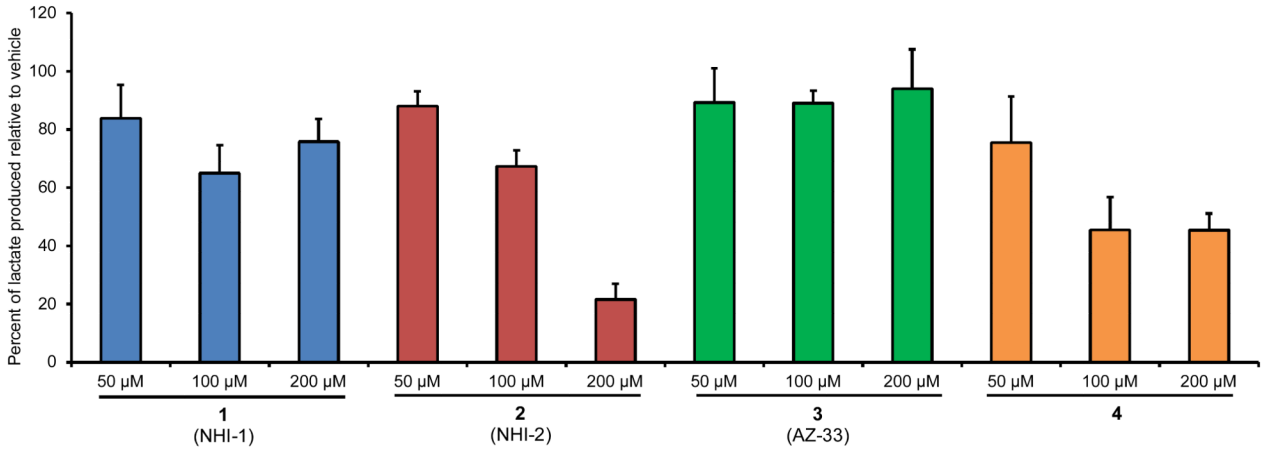

Fig 4.

Lactate production inhibition in HeLa cells quantified by GC-MS. HeLa human cervical carcinoma cells were treated with 50-200 μM concentrations of each compound for 8 hours. Cell culture media was extracted from each treatment, concentrated, and derivatized for GC-MS detection and quantification of lactate. Error bars denote standard error (n≥3 independent experiments).

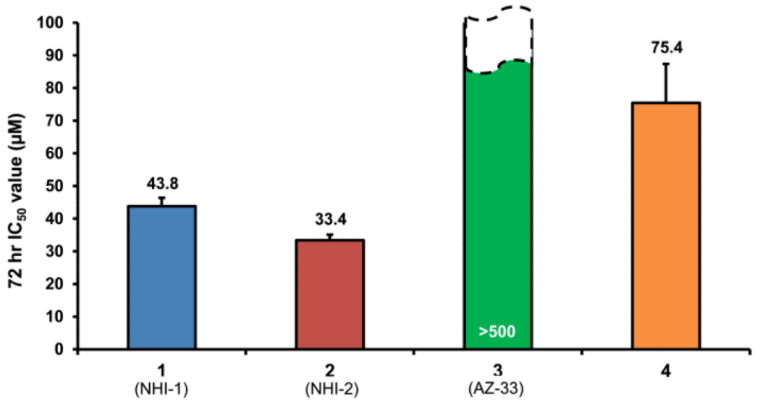

Fig 5.

Anticancer potencies (shown here as 72 hour IC_{50}values) of **1**-**4** in HeLa human cervical carcinoma cells. Error bars denote standard error (n≥3).

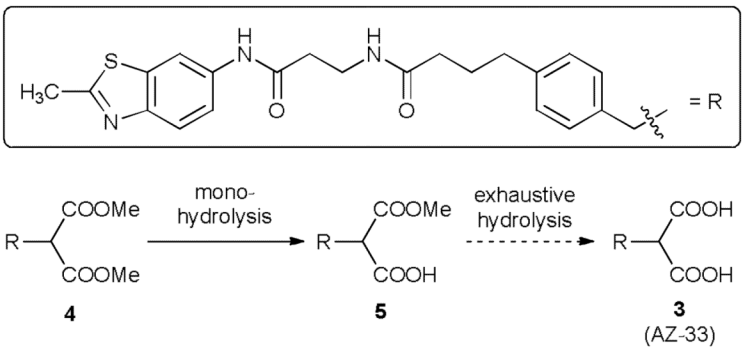

Scheme 1.
Putative transformations of Mal derivative 4 upon entrance into HeLa cells.

Table 1

Enzyme inhibition potencies (IC_{50})

Cpd	LDH-A (IC_{50}, μM)[a]		LDH-B (IC_{50}, μM)[a]	
	[NADH][b]	[Pyr][c]	[NADH][b]	[Pyr][c]
1	29.0 ± 3.0	73.4 ± 11.0	123.8 ± 0.7	> 200
2	14.7 ± 2.1	10.5 ± 2.5	55.8 ± 7.1	53.8 ± 4.4
3	0.54 ± 0.03	1.0 ± 0.2	3.6 ± 0.4	5.0 ± 0.8
4	> 200	> 200	> 200	> 200
5	4.8 ± 1.0	22.7 ± 3.3	26.9 ± 3.0	106 ± 11

[a] Values are reported as the mean ± SD of three or more independent experiments.

[b] NADH-competition assay: saturating concentration (1440 μM) of sodium pyruvate and competitive concentration (40 μM) of NADH.

[c] Pyruvate-competition assay: saturating concentration (150 μM) of NADH and competitive concentration (200 μM) of sodium pyruvate.